Investigation of Interporphyrin Charge Resonance of Dihedral Angle Controlled Porphyrin Dimers by Resonance Raman Spectroscopy and MO Approaches

Dae Hong Jeong, Sung Moon Jang, In-Wook Hwang, and Dongho Kim*

Center for Ultrafast Optical Characteristics Control and Department of Chemistry, Yonsei University, Seoul 120-749, Korea

Naoya Yoshida and Atsuhiro Osuka*

Department of Chemistry, Graduate School of Science, Kyoto University, Kyoto 606-8502, Japan

Received: June 18, 2002; In Final Form: August 26, 2002

Strongly interacting porphyrin dimers as a form of cofacial or side-to-side linkage have been ideally suited for investigation on the structure−electronic property relationship in porphyrin dimers. The relative orientation and interchromophore distance determined by the dihedral angle between the two porphyrin units are key factors in controlling the interchromophoric interaction. In the present work, directly linked porphyrin dimers with a systematic change in the dihedral angle between the two porphyrin planes have been investigated by resonance Raman (RR) and emission spectroscopies. Extremely strong molecular orbital interactions between the porphyrin units by decreasing the dihedral angle give rise to strongly enhanced interporphyrin charge-resonance transitions. With a decrease of the dihedral angle, unique RR spectra of the porphyrin dimers were also observed depending on the excitation wavelengths of 406.7, 457.9, and 488.0 nm. With the aid of supermolecular MO approaches it was found that the charge-resonance band at ca. 450 nm involves $a_{1u}{}^{A} \rightarrow (1/\sqrt{2})(e_{gx}+e_{gy})^{B}$ transition. Upon excitation at this transition, the Raman modes involving $\nu(C_\alpha C_\beta)$ and $\nu(C_\beta C_\beta)$ motions such as ν_{38}, ν_{11}, and ν_3 are predominantly enhanced. The MO calculation also revealed a considerable mixing between the charge-resonance transition and the excitonic transition with a decrease of the dihedral angle. The fast component in the fluorescence decay (ca. 500 ps) was found to increase in its contribution as the dihedral angle decreases, which was tentatively interpreted in terms of the vibronic mixing of the Q-band mixed with the charge-resonance transition.

I. Introduction

Optical and electronic properties of a variety of porphyrin arrays have aroused much scientific interest owing to their potential applications as solar cell, molecular photonic and electronic devices.[1−3] The recent success in elaborating various porphyrin architectures using several types of linkers via meso position attachment has enabled systematic studies of structure−property relationships.[1−11] Molecular rods may be used to place two active centers at a known distance apart and connect them by a medium of known structure. The degree of interaction between the centers must depend on the electronic structure of the rod and the structural displacement between them, such as interchromophore distance and orientation. Recently, it became possible to synthesize directly meso−meso linked porphyrin arrays, which exhibit unusually strong exciton splitting in their Soret bands due to a short center-to-center distance (∼8.35 Å).[12,13] The directly meso−meso linked linear porphyrin arrays always have shown predictable changes in optical properties according to Kasha's exciton model. Their $S_2 \rightarrow S_1$ internal conversion rates have been accelerated through opening a ladder-type deactivation channel arising from the low-energy exciton split band as a function of the porphyrin array length. Another distinct feature of this molecular system is that their interchromophoric electronic interactions are nearly free from π-conjugation due to their orthogonal conformation caused by the direct linkage between the adjacent porphyrin rings. Because not only the interporphyrin distance but also the dihedral angle are important in determining electronic interactions in the porphyrin arrays, it is relevant to investigate how the dihedral angle between the neighboring porphyrins influences the electronic nature of the porphyrin arrays.

The electronic properties of the dihedral angle-controlled diporphyrins[14] exhibited new absorption bands appearing at 390 and 450 nm and an excitonic Soret band shifting from 450 to 480 nm with a decrease of the dihedral angle. Based on MO calculations, the new bands at 390 and 450 nm are characterized as charge-resonance transitions and the shifted excitonic Soret band is strongly affected by orbital interactions between the two porphyrin planes. The weak band at 450 nm is not fully characterized due to its weakness in intensity. Its position between the strong excitonic Soret transitions may give rise to strong vibronic interaction with them. As the charge-resonance and excitonic transitions are intrinsically different from each other in their electronic properties, the resonance Raman spectroscopy can be utilized in discerning the electronic nature of the transition by monitoring the RR enhancement pattern depending on the excitation wavelength.[15−20] In the present study, we have performed the RR spectroscopic experiments to explore the electronic nature of the electronic transitions of the dihedral angle-controlled diporphyrins. To describe the mixing between the charge-resonance and excitonic transitions in a detailed manner, we have also carried out simple super-

* Corresponding authors.

10.1021/jp021439b CCC: $22.00
Published on Web 10/26/2002

SCHEME 1: Molecular Structures of the Porphyrin Dimers, S*N*s (where *N* is the number of carbons in the strapping chain)

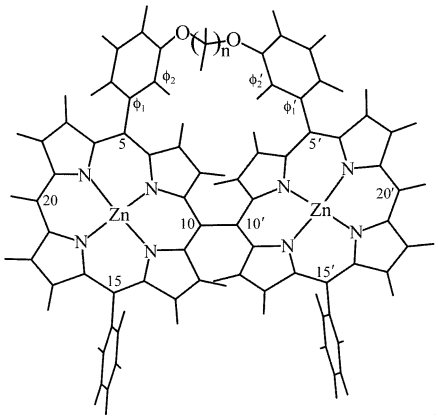

molecular MO approaches. Based on the MO calculations, the RR enhancement as well as the interaction between the charge-resonance and excitonic transitions has been addressed.

II. Experiemental Section

Zn(II) 5,15-bis(3,5-dioctyloxyphenyl)porphyrin (Z1), and its meso,meso-linked porphyrin arrays from dimer (Z2) were synthesized through repetitive Ag^{I}-promoted meso,meso-coupling reactions.[12,13] The dihedral angle controlled dimers were synthesized by linking the peripheral phenyl group with a strapping chain of different length (we denote the strapped porphyrin dimer as S*N*, $N = 1$, 2, 3, 4, 8, and 10; *N* is the number of carbon atoms in the chain) (Scheme 1). Recycled GPC−HPLC was used for product separation. MALDI-TOF mass and ^{1}H NMR spectra were employed for product characterization. The spectroscopic grade tetrahydrofuran (THF) was used as a solvent for all experiments.

The absorption spectra were recorded by using a Varian Cary 3 spectrophotometer, and fluorescence measurements were made on a scanning SLM-AMINCO 4800 spectrofluorometer, which makes it possible to obtain the corrected fluorescence spectra using Rhodamine B as a quantum counter. Steady-state fluorescence excitation anisotropy spectra were obtained by changing the detecting polarization in the fluorescence path parallel or perpendicular to the polarization of the exciting light. Then anisotropy values were calculated as follows:

$$r = \frac{I_{VV} - GI_{VH}}{I_{VV} + 2GI_{VH}}$$

where I_{VV} (or I_{VH}) is the signal intensity when the excitation light is vertically polarized and only the vertically (or horizontally) polarized portion of fluorescence is detected, denoting that the subscripts stand for excitation and detection polarization, respectively. The factor G defined by I_{HV}/I_{HH} corresponds to the ratio of the sensitivities of the detection system for vertically and horizontally polarized light.

Picosecond time-resolved fluorescence experiments were carried out by using the time-correlated single photon counting (TCSPC) method.[21] The picosecond excitation pulses were obtained from a cavity-dumped picosecond dye laser (Coherent 702) synchronously pumped by a mode-locked Nd:YAG laser (Coherent Antares 76-s). The cavity-dumped beam from the dye laser has 2 ps pulse width and an average power of ca. 40 mW at 3.8 MHz dumping rate when Rhodamine 6G as the gain dye was used. The emission was collected at 45° with respect to the excitation laser beam by 5- and 25-cm focal length lenses, focused onto a monochromator (Jobin-Yvon HR320), and detected with a microchannel plate photomultiplier tube (Hamamatsu R2809U). The signal was amplified by a wideband amplifier (Philip Scientific), sent to a Quad constant fraction discriminator (Tennelec), a time-to-amplitude converter (Tennelec), a counter (Ortec), and a multichannel analyzer (Tennelec/Nucleus), and stored in a computer.

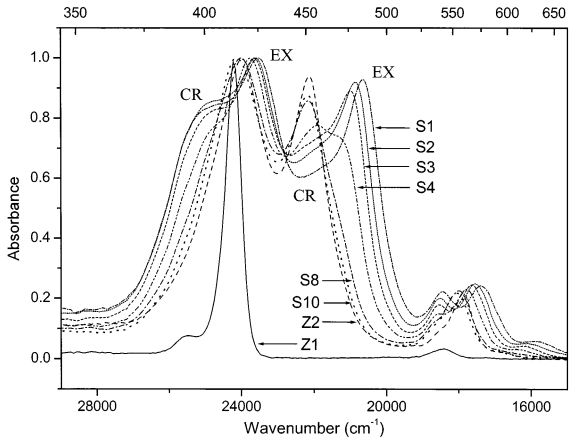

Figure 1. A series of normalized ground-state absorption spectra of porphyrin monomer (Z1), orthogonal dimer (Z2), and strapped dimers (S*N*s) dissolved in THF. EX and CR represents excitonic and charge-resonance characters, respectively.

The ground-state resonance Raman spectra of the strapped porphyrin dimers were obtained by photoexcitation using two lines (457.9 and 488.0 nm) of a cw Ar ion laser (Coherent INNOVA 90) and 406.7 nm line of a cw Kr ion laser (Coherent INNOVA 70K). These lines correspond to the low-energy exciton split Soret bands and the high-energy Soret band of the strapped porphyrin dimers. Raman scattering signals were collected in a 90° scattering geometry. Various Raman detection systems were used such as a 1-m double monochromator (ISA Jobin-Yvon U-1000) equipped with a thermoelectrically cooled photomultiplier tube (Hamamatsu R943-02), a single pass spectrograph (Acton Research 500i) equipped with a charge-coupled device (PI LN/CCD-1152E).

III. Results

Steady-State Absorption and Fluorescence Spectra. The absorption spectra of Z2, S*N*s and their constituent monomer (Z1) are shown in Figure 1. Because *N* represents the number of carbons in the strapping chain, the dihedral angle between the porphyrin moieties decreases as *N* decreases. The absorption spectra of S*N*s denote unique features in their electronic structures depending on the dihedral angle. As the dihedral angle decreases from 90°, the $\pi-\pi$ interaction between the porphyrin units gradually increases, resulting in new features unpredicted by the exciton coupling model. The high-energy band at ca. 415 nm gradually splits into the two bands at ca. 390 and 425 nm as the strap length decreases, in which the higher-energy band at ca. 390 nm exhibits charge-resonance (CR) character and the lower-energy band at ca. 425 nm excitonic (EX) nature. The low-energy split band at 450 nm becomes gradually red-shifted up to 480 nm, and a weak band contributing to the absorption at around 450 nm can be noticed as the dihedral angle decreases. The lower-energy band shifted up to 480 nm was considered to possess excitonic character and the nearby moderate band at 450 nm to denote a charge-resonance feature.

The systematic changes in the absorption spectra of the dimers are reflected in their corresponding fluorescence spectra. Figure

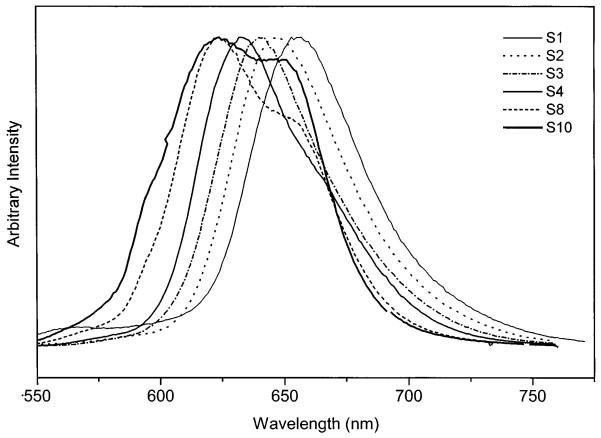

Figure 2. A series of normalized fluorescence spectra of strapped porphyrin dimers (S*N*s) in THF with an excitation at 415 nm.

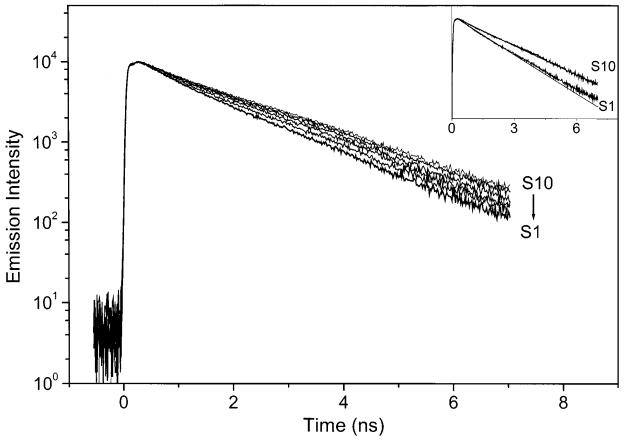

Figure 3. Fluorescence decay profiles of strapped porphyrin dimers (S*N*s) in THF observed at 655 nm after photoexcitation at their corresponding Q-bands. The inset shows the fluorescence decay curves of S1 and S10 with a single-exponential decay as a guide for eye.

2 shows the fluorescence spectra of S*N*s with an excitation at ca. 415 nm. As the strap chain becomes short, the fluorescence bands become merged into one band to the red side at ca. 660 nm. This band mainly originates from the Q(0,0) band (ca. 630 nm) showing a consistent red-shift as in the absorption spectra. Fluorescence decay profiles of the strapped porphyrin dimers at 655 nm were monitored after photoexcitation at their corresponding Q bands (Figure 3). Gradual decrease of the fluorescence decay times was observed in going from S10 to S1. The inset in Figure 3 shows the fluorescence decay profiles of S10 and S1 and their fitted curves with a single exponential decay function. This reveals that the decay profile of S1 deviates from a single exponential decay while that of S10 roughly follows a single-exponential decay. The decay curves were successfully fitted with double exponential decay functions for all strapped dimers, and the resulting time constants are summarized in Table 1. While the time constant for the slow component is comparable to the fluorescence lifetime (1.94 ns) of Z2, the fast component of ca. 400 ps was not detected for Z2.[22] The fast component shows little change in going from S10 to S3 and becomes slightly slower in S2 and S1. On the other hand, the time constant for the slow component gradually decreases from 1.90 to 1.57 ns in going from S10 to S1, respectively. The relative contribution of the fast component in fluorescence intensity is about 10% from S10 to S3 but increases up to 26% in going from S2 to S1.

TABLE 1: Fluorescence Decay Lifetimes of S*N*s Observed at 655 nm after Photoexcitation at Their Corresponding Q-bands

	fast component		slow component	
	τ_1	intensity ratio[a]	τ_2	intensity ratio
S1	0.59	26%	1.57	74%
S2	0.46	17%	1.62	83%
S3	0.38	9.9%	1.67	90.1%
S4	0.35	9.1%	1.74	90.9%
S8	0.41	9.9%	1.84	90.1%
S10	0.39	10.7%	1.90	89.3%

[a] Amplitude ratio between species 1 and species 2.

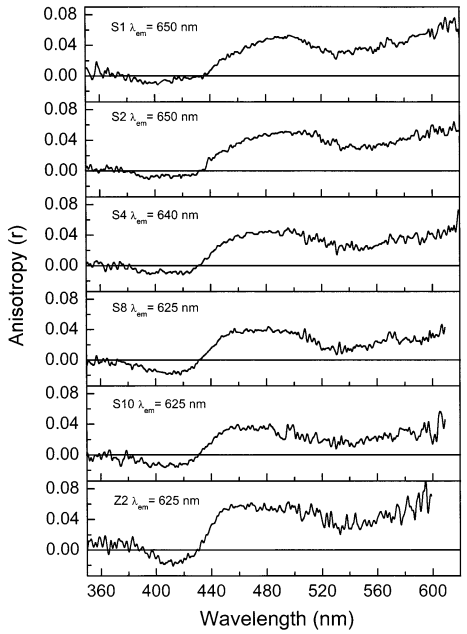

Figure 4. A series of steady-state fluorescence excitation anisotropy spectra of strapped porphyrin dimers (S*N*s) in THF monitored at their fluorescence maximum positions.

Steady-state absorption/fluorescence polarization anisotropy experiments were performed in order to gain further insight into the relative orientation between absorption and emission dipoles in the porphyrin dimers (Figure 4). The bottom curve in Figure 4 represents the characteristic anisotropy features of the orthogonal porphyrin dimer such that the high-energy Soret band at 415 nm has negative anisotropy values and the low-energy band at 450 nm has positive values similar to the Q-band region (the region close to 600 nm). As expected from the absorption spectrum, the fluorescence excitation anisotropy spectrum of S10 is similar to that of Z2. The overall pattern of the fluorescence excitation anisotropy spectra is nearly the same for all S*N*s, except that the negative contribution at 415 nm decreases and the positive maximum at around 460 nm shifts to red in going from S10 to S1. By the negative anisotropy at 415 nm with a decrease of the strap chain length, it can be considered that the direction of transition dipole at 415 nm is not sharply defined in the strapped porphyrin dimers due to the reduced symmetry from D_{4h} of porphyrin monomer caused by severe structural deformation. The positive value at around 460 nm indicates that the transition dipole of the corresponding absorption band is parallel with that of the lowest excited state from which fluorescence emits.

Resonance Raman Specra of S*N*s. Resonance Raman (RR) spectra of S*N*s ($N = 1$, 2, 3, 4, 8, and 10) and Z2 are shown in Figure 5. The 457.9 and 488.0 nm Ar^+ ion laser lines were

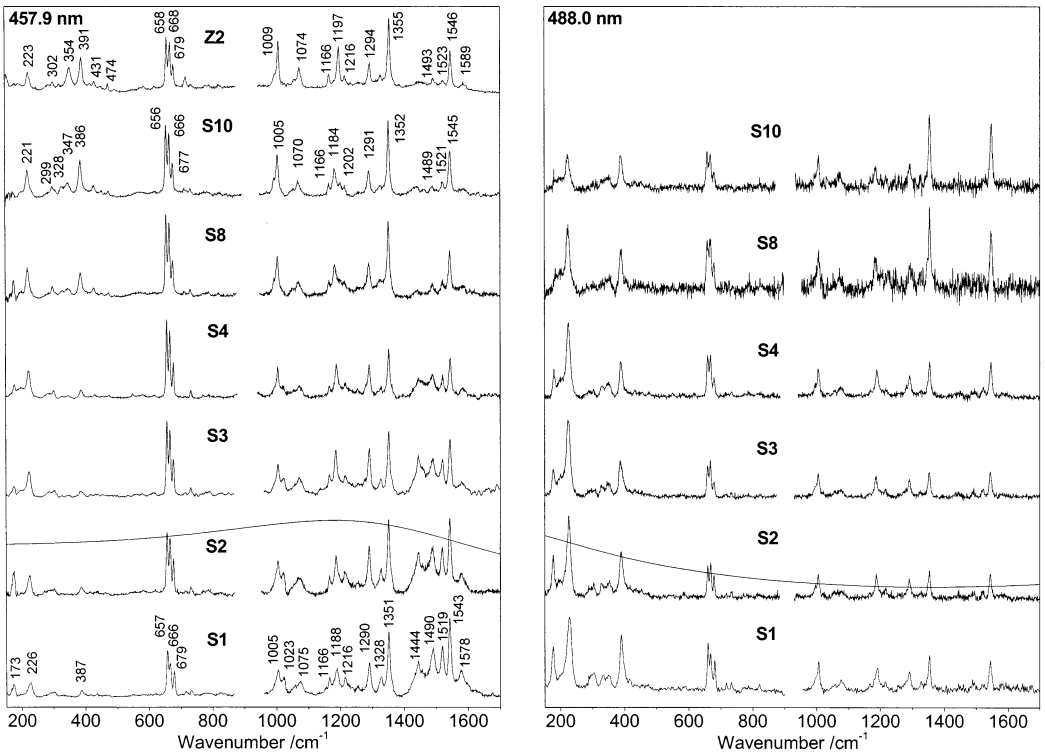

Figure 5. Resonance Raman spectra of orthogonal dimer (Z2) and strapped dimers (S*N*s) in THF from top to bottom by excitation at 457.9 nm (left column) and those of S*N*s by excitation at 488.0 nm (right column). The absorption spectra of S2 corresponding to the spectral regions of the RR spectra of S2 are drawn overlapping to check the influence of self-absorption on Raman intensities.

selected as Raman excitation lines in order to elucidate the electronic nature of the absorption bands in 430−500 nm region. The RR spectrum of S10 by photoexcitation with the 457.9 nm laser line is nearly the same as that of Z2, exhibiting the dominant enhancement of the Raman bands at 1545, 1352, 1291, 1184, 1070, 1005, 386, and 221 cm^{-1} and the triple bands at around 666 cm^{-1}. They all correspond to the totally symmetric A_1 modes under the D_{2d} symmetry point group of the orthogonal porphyrin dimer Z2. The Raman bands at 1545, 1352, 1070, 1005, and 386 cm^{-1} in the RR spectrum of S10 are attributed to the ν_2, ν_4, ν_9, ν_6, and ν_8 modes of the porphyrin monomer.[23,24] The large enhancement of the triple bands at around 666 cm^{-1} that originate from $C_\alpha C_m C_\alpha$ bending vibration (ϕ_9 mode) is also observed. The Raman bands at 1291, 1184, and 221 cm^{-1} are assigned to the symmetric combination modes of the ν_{27}, ν_{51}, and ν_{35} modes of the porphyrin monomer. These spectral features are characteristic of the directly linked porphyrin dimer with orthogonal geometry in the case of the low-energy Soret excitation. In going from S10 to S1, however, the RR enhancement pattern shows systematic changes. The Raman bands at 1023, 1444, 1490, and 1519 cm^{-1} become gradually stronger, and the low-frequency bands such as the ν_8 mode at 387 cm^{-1} lose their intensities. One may think that the variations in RR intensities reflect the differences in the absorption bands. However, the absorption spectra of S2 overlapping with the RR spectra, for instance, clearly indicate that the self-absorption in Raman signals does not affect the RR enhancement (Figure 5).

The RR spectra of S*N*s by photoexcitation with the 488.0 nm laser line reveal totally different features than those by photoexcitation with the 457.9 nm laser line in going from S10 to S1. They all show nearly the identical RR enhancement pattern by the 457.9 nm excitation except a large enhancement of the low-frequency modes below 500 cm^{-1} and the diminishment of the RR bands at 1023, 1444, 1490, 1519, and 1578 cm^{-1} with a decrease of the dihedral angle. Most of the RR bands are attributed to the totally symmetric modes spanning the A_1 symmetry under the D_{2d} point group of the orthogonal porphyrin dimer Z2 such as the RR bands of S10 by photoexcitation with the 457.9 nm laser line. They all originate from the A_{1g}, B_{2g} and E_u modes of the porphyrin monomer. The overall mode assignments of the RR bands are given in Table 2 based on the normal-mode analysis of Z2.[24] A major difference in the RR enhancement by 457.9 and 488.0 nm excitation is regarded to arise from the different electronic properties of the corresponding absorption transitions.

A slight shift in vibrational frequency is observed for some Raman bands (Table 3). While the ν_2, ν_{38}, and ϕ_4 modes show decrease in frequency, the ν_9 and ν_{35} modes are shifted to higher frequency with a decrease of the dihedral angle. The other bands such as ν_4, ν_1, ϕ_9, and ν_8 modes are relatively less affected by the dihedral angle change. It is interesting to note that most of the RR bands shifting to red or blue are contributed by the $\nu(C_\alpha C_\beta)$ and/or $\nu(C_\beta C_\beta)$ modes except the ν_{35} mode. The ν_{35} mode is directly affected by the geometric distortion caused by the strapping chain. This mode is believed to be one of the direct probes for geometric parameters related to the phenyl linkage. The other modes are regarded as reflecting the geometric changes, especially occurring in porphyrin planes. Considering the extent of frequency shifts, however, the dihedral angle change does not seem to significantly affect the vibrational force constants. The enhancement of the low-frequency Raman modes below 400 cm^{-1} by 488.0 nm excitation in going from S10 to S1 is worthy of being mentioned. Previously we observed the similar RR enhancement pattern in the low-frequency region by excitation at the low-energy excitonic Soret bands of the orthogonal porphyrin arrays as the length of the orthogonal porphyrin arrays increased.[24] These features along with the invariant RR enhancement pattern from S10 to S1 by the 488.0

TABLE 2: Normal Mode Assignment of the RR Bands of Strapped Porphyrin Dimer (S10 and S1)

S10 (cm^{-1})	S1 (cm^{-1})		local coordinate of porphyrin monomer[a]	symmetry
~175	173	ν_{35}	ν(Pyr-transl) phenyl moving	$B_2(B_{2g})$[b]
221 (0.3)[c]	226 (0.36)[d]	ν_{35}	ν(Pyr-transl) phenyl moving	$A_1(B_{2g})$
347 (0.31)		ϕ_{10}	$\nu(C_m\text{-}C_{Ph})$ phenyl moving	$A_1(A_{1g})$
386 (0.30)	387 (0.34)	ν_8	$\nu(NM) + \delta(C_\alpha NC_\alpha) + \nu(C_\alpha C_m)$	$A_1(A_{1g})$
429 (0.39)		ν_{33}	$\delta(C_\alpha C_m) + \nu(C_\alpha C_m) + \nu(C_\alpha C_\beta)$	$A_1(A_{1g})$
656 (0.33)	657 (0.27)	ϕ_9	$\delta(C_\alpha C_m C_\alpha) + \nu_{6a}$(Ph)	$A_1(A_{1g})$
677 (0.29)	679 (0.27)			$B_2(A_{1g})$
666 (0.31)	666 (0.33)	ϕ_9''	$\delta(C_\alpha C_m C_\alpha) + \nu_{6a}$(Ph)	$A_1(E_u)$
1005 (0.28)	1005 (0.43)	ν_6	$\nu(NC_\alpha) + \nu(C_\alpha C_\beta)$	$A_1(A_{1g})$
	1023	ν_{22}	$\nu(C_\alpha C_\beta) + \nu(NC_\alpha) + \delta(C_\beta H)$	$E(A_{2g})$
1070 (0.31)	1074	ν_9	$\delta(C_\beta H) + \nu(C_\beta C_\beta)$	$A_1(A_{1g})$
1166 (0.28)	1166 (0.38)	ν_{34}	$\delta(C_\beta H) + \nu(C_\alpha C_\beta)$	$A_1(B_{2g})$
1184 (0.26)	1188 (0.30)	ν_{51}	$\delta(C_\beta H) + \nu(C_\beta C_\beta)$	$A_1(E_u)$
1215 (0.31)	1215 (0.37)	ν_1	$\nu(C_m C_{phenyl}) + \nu(NC_\alpha)$	$A_1(A_{1g})$
1291 (0.33)	1290 (0.43)	ν_{27}	$\nu(NC_\alpha) + \nu(C_m C_{phenyl})$	$A_1(B_{2g})$
1327 (0.65)	1328 (0.56)	ν_{29}	$\nu(C_\alpha C_\beta) + \nu(C_\beta H)$	$A_1(B_{2g})$
1352 (0.32)	1351 (0.51)	ν_4	$\nu(C_\alpha C_\beta) + \nu(NC_\alpha) + \delta(C_\alpha NC_\alpha) + \delta(C_\alpha C_m)$	$A_1(A_{1g})$
1443 (0.47)	1444 (0.58)	ν_3	$\nu(C_\alpha C_m) + \nu(C_\beta C_\beta)$	$A_1(A_{1g})$
1489 (0.72)	1490 (0.71)	ν_{11}	$\nu(C_\beta C_\beta) + \delta(C_\beta H)$	$E(B_{1g})$
1521 (0.51)	1519 (0.59)	ν_{38}	$\nu(C_\alpha C_m) + \nu(C_\beta C_\beta) + \nu(CC)_{Ph}$	$A_1(E_u)$
1545 (0.30)	1543 (0.54)	ν_2	$\nu(C_\beta C_\beta)$	$A_1(A_{1g})$
1584 (0.72)	1578 (0.79)	ϕ_4/ϕ_4''	$\nu(C_m\text{-}C_{Ph}) + \nu_{8a}$(Ph) + $\nu(C_\beta C_\beta)$	$A_1(A_{1g})/A_1(E_u)$

[a] The notations for normal classification are adapted from ref. 23. [b] Symmetry block in D_{4h} symmetry. [c] Numbers in parentheses are the depolarization ratios for S10. [d] Numbers in parentheses are the depolarization ratios for S2 instead of S1.

TABLE 3: Vibrational Frequencies of Resonance Raman Modes of S*N*s

	Raman frequencies (cm^{-1})						
modes	Z2	S10	S8	S4	S3	S2	S1
ν_{35}	223	221	220	222	224	225	226
ϕ_{10}	354	347					
ν_8	391	386	387	387	386	388	387
ν_{33}	431	429	429	430			
ϕ_9	658	656	656	657	657	657	657
	679	677	677	678	677	677	679
ϕ_9''	668	666	666	667	666	666	666
ν_6	1009	1005	1005	1005	1006	1004	1005
ν_{22}					1021	1022	1023
ν_9	1074	1070	1071	1073	1073	1073	1074
ν_{34}	1166	1166	1166	1168	1166	1166	1166
ν_{51}	1197	1184	1184	1188	1187	1187	1188
ν_1	1215	1215	1216	1216	1216	1215	1215
ν_{27}	1294	1291	1290	1291	1291	1290	1290
ν_{29}	1328	1327	1328	1328	1327	1327	1328
ν_4	1355	1352	1351	1352	1352	1351	1351
ν_3		1443	1443	1444	1444	1444	1444
ν_{11}	1493	1489	1489	1488	1491	1490	1490
ν_{38}	1523	1521	1521	1521	1521	1519	1519
ν_2	1546	1545	1544	1545	1544	1543	1543
ϕ_4/ϕ_4''	1587	1584	1584	1580	1580	1578	1578

nm laser line excitation allow us to confirm that the absorption band of S1 at 478 nm possesses the excitonic nature. The gradual enhancement of the Raman bands at 1023, 1444, 1490, and 1519 cm^{-1} with 457.9 nm excitation in going from S10 to S1 implies that the electronic nature of the corresponding transition is quite different from the red-shifted excitonic band at around 480 nm. The absorption band at around 450 nm is believed to be due to charge-resonance transition based on the MO calculations.

We also measured the depolarization ratios of the RR modes of S10 and S2 as the two extreme cases of the dihedral angle change. S10 represents almost identical features to Z2, giving the depolization ratios of around 0.3. In the case of S2, the depolarization ratios exhibit complicated trends. Some of the RR bands observed by 488.0 nm excitation exhibit the increased depolarization ratio values up to ca. 0.5 (Table 2). The increase of the depolarization ratio is easily expected by the fact that the Raman tensor is perturbed by symmetry change from D_{2d} to D_2. The RR bands at 1490, 1519, and 1578 cm^{-1} enhanced only by 457.9 nm excitation show large ρ values close to 0.75, while the RR band at 1444 cm^{-1} (ν_3 mode) shows $\rho \approx 0.5$. The large ρ value close to 0.75 implies that these bands can be attributed to depolarized vibration modes.

In the case of the porphyrin dimer with orthogonal geometry, the resonance Raman spectrum by photoexcitation at the high-energy Soret band revealed monomer-like spectral features, which are caused by a negligible interaction between the Soret transitions perpendicular to the long molecular axis.[22,24] In strapped porphyrin dimers, however, as the strap length decreases, the interaction of the Soret transitions becomes pronounced. To probe the spectral changes caused by the dihedral angle variation, we also observed the RR spectra of S*N*s with photoexcitation at the high-energy Soret band. As shown in Figure 6 the RR spectra of the S*N*s obtained by photoexcitation at 406.7 nm are nearly the same, irrespective of the dihedral angle change. The RR spectra exhibit spectral features characteristic of porphyrin monomers such that while the ν_2, ν_4, ν_9, ν_6, and ν_8 modes appear clearly, the ν_{27}, ν_{34}, ν_{51}, and ϕ_9 modes characteristic of the directly linked porphyrin dimer are not enhanced.

IV. Discussion

Steady-State Absorption Spectra. The direct linkage of two porphyrin units gives rise to unique properties such as strong excitonic interactions due to a close proximity. In the case of the porphyrin dimer, Z2, without a strap chain the porphyrin planes maintain an averaged orthogonal geometry due to steric repulsion between the two porphyrins. This feature allows the successful application of the exciton model to this closely linked diporphyrin, giving one red-shifted excitonic Soret band (B_2 symmetry in D_{2d} point group) and two degenerate monomer-like Soret bands (E symmetry). However, strong interaction between closely facing orbitals could not be totally precluded. This was reflected in the significant broadening of the excitonic bands[22] and the considerable contribution of charge-resonance character in the low-energy excitonic Soret band.[25] When the dihedral angle was reduced, the latent features of interporphyrin

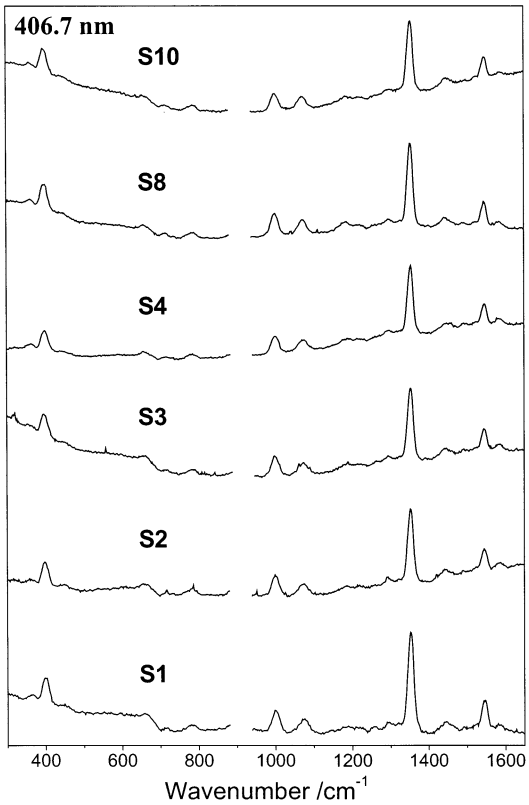

Figure 6. Resonance Raman spectra of strapped porphyrin dimers (S*N*s) in THF by excitation at the high-energy Soret band using 406.7 nm line from a Kr ion laser.

MO interactions began to appear. Specifically, the low-energy exciton Soret band (B_2 in D_{2d} group and B_1 in D_2 group), which should not be shifted according to the exciton model, was red-shifted by ca. 30 nm while a new band (B_2 in D_{2d} group and B_1 in D_2 group), assigned as a charge-resonance transition, appeared at ca. 450 nm. The high-energy Soret band at 415 nm was split by excitonic interactions, but still remained as one band overlapped with each other due to weak interactions (E in D_{2d} group and B_2/B_3 in D_2 group). The new band appearing at 390 nm was assigned as a charge-resonance transition.

The Raman enhancement of vibrational modes is strongly affected by the electronic transition where the Raman excitation line lies. The similar RR enhancement pattern of S1 by 488.0 nm excitation to that of Z2 demonstrates that the absorption band at 480 nm has mostly excitonic character originating from the low-energy excitonic Soret transition of Z2 at 450 nm. Different RR enhancement pattern of S1 with photoexcitation at 457.9 nm reveals that the electronic transition in this region has different electronic property from the excitonic Soret band, supporting the assignment of charge-resonance transition. It is also noteworthy that despite the difference in the RR enhancement by 457.9 and 488.0 nm excitations, the Raman spectrum of S1 with excitation at 457.9 nm has mostly common features with that of Z2, indicating that the corresponding transition is considerably mixed with excitonic character.

Supermolecular MO Approach. To clarify the mixing of charge-resonance and excitonic transitions we adopted simple supermolecular MO approaches. The supermolecular MO approaches have been utilized to describe the optical properties of various dimer complexes including sandwich porphyrin complexes, bateriochlorin dimer and the reaction center special pair. Using eight HOMOs and LUMOs of two porphyrin units, the MOs of the porphyrin dimer were constructed under D_2 symmetry (and also under D_{2d} and D_{2h}) as follows (Figure 7):

$(a_{1u}^A - a_{1u}^B)/2^{1/2}$	→	$1a_2$ (D_{2d})	$1b_1$ (D_2)	$1b_{1g}$ (D_{2h})
$(a_{1u}^A + a_{1u}^B)/2^{1/2}$	→	$1b_1$	1a	$1a_u$
$(a_{2u}^A + a_{2u}^B)/2^{1/2}$	→	$1e_x$	$1b_3$	$1b_{3u}$
$(a_{2u}^A - a_{2u}^B)/2^{1/2}$	→	$1e_y$	$1b_2$	$1b_{2g}$
$(e_{gx}^A + e_{gy}^A + e_{gx}^B + e_{gy}^B)/2$	→	$2a_2$	$2b_1$	$2b_{1g}$
$(e_{gx}^A + e_{gy}^A - e_{gx}^B - e_{gy}^B)/2$	→	$2b_1$	2a	$2a_u$
$(e_{gx}^A - e_{gy}^A - e_{gx}^B + e_{gy}^B)/2$	→	$2e_x$	$2b_3$	$2b_{3u}$
$(e_{gx}^A - e_{gy}^A + e_{gx}^B - e_{gy}^B)/2$	→	$2e_y$	$2b_2$	$2b_{2g}$

For the following description we adopted a new axis convention in which the longest axis of dimer is denoted as *Z*-axis, the one that is perpendicular to the *Z*-axis and bisecting the dihedral angle is as *Y*-axis, and the other is as *X*-axis (Figure 7). The *x*- and *y*-axes are the same as the conventional ones used for the MO description of porphyrin monomers.[26] The *x*′- and *y*′-axes are used for an auxiliary purpose. The orbital energy splittings are calculated by the effective one-electron Hamiltonian (H_{eff}) and the Hamiltonian used in the configuration interaction is $H = H_{\text{eff}} + \Sigma e^2/r_{ij}$. Only singly excited configurations are considered in describing the electronic states of the porphyrin dimer. In deducing the singlet excited states there are 12 dipole-allowed configurations. Four configurations have B_1 symmetry that spans the *Z* direction of the dimer, another four configurations have B_2 symmetry with *Y* direction, and the remaining four configurations have B_3 symmetry with *X* direction. In

B_1 symmetry (*Z*):	$1b_1 \rightarrow 2a$	$1b_2 \rightarrow 2b_3$	$1a \rightarrow 2b_1$	$1b_3 \rightarrow 2b_2$
B_2 symmetry (*Y*):	$1b_1 \rightarrow 2b_3$	$1b_2 \rightarrow 2a$	$1a \rightarrow 2b_2$	$1b_3 \rightarrow 2b_1$
B_3 symmetry (*X*):	$1b_3 \rightarrow 2a$	$1a \rightarrow 2\,b_3$	$1b_2 \rightarrow 2a_2$	$1a_2 \rightarrow 2b_2$

presenting the most mathematically tractable form of the model, we follow the calculations on other dimers,[27−30] neglect differential overlap, and also adopt a cyclic polyene approximation.[27] The calculations are performed in the case of $\theta = 90°$

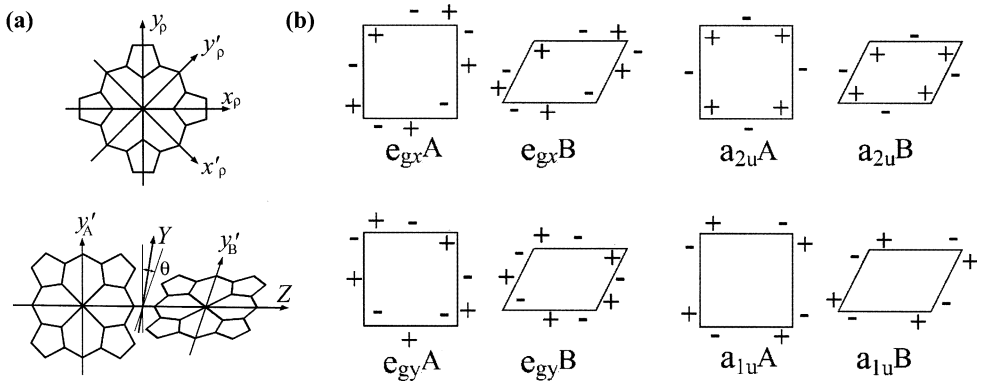

Figure 7. Axis definition used for MO description (a), and eight HOMOs and LUMOs of two porphyrin units used for the basis constructing the supermolecular MOs of the porphyrin dimer (b).

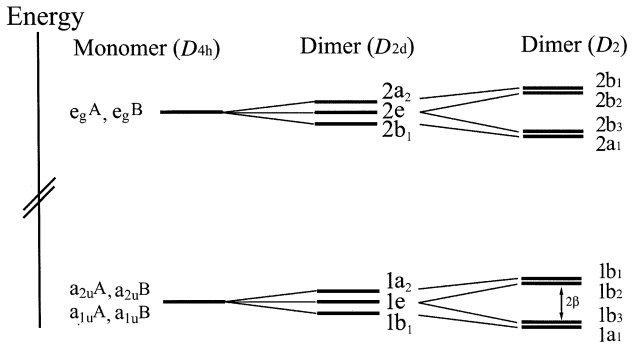

Figure 8. Simplified energy levels of molecular orbitals. The relative spacing of the energy levels is exaggerated.

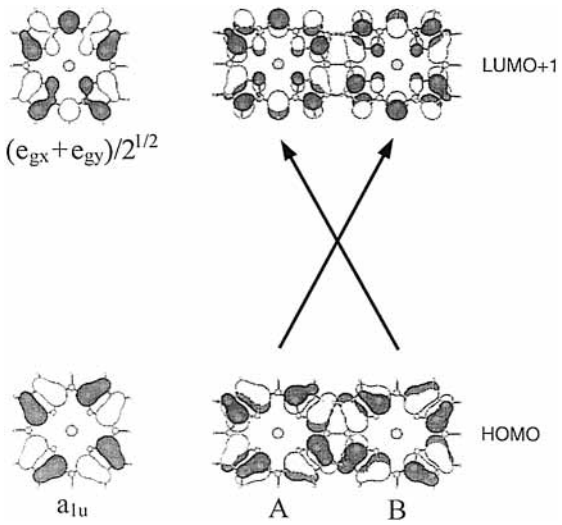

Figure 9. MO pictures of the a_{1u} and $(e_{gy}+e_{gx})/\sqrt{2}$ orbitals depicting charge transfer from porphyrin unit A to porphyrin unit B and vice-versa.

and $\theta \neq 90°$. For $\theta = 90°$ the constituent porphyrin planes are orthogonal to each other and hence the resonance integrals between the bonding and antibonding MOs are assumed to be negligible ($\beta \approx 0$). For $\theta \neq 90°$, all resonance integrals are assumed to be $\beta \neq 0$ (Figure 8). Then, even though very simplified in mathematical treatment, we can obtain functional expressions predicting six allowed exciton transitions (B- and Q-bands) and six charge-resonance terms (Tables 4 and 5).

Table 4 illustrates that the excitonic and charge-resonance characters are well separated when $\theta = 90°$. The energies of CT_1 and CT_2 transitions are expressed as degenerate. Examining carefully the CT_{1Z} transition appearing at 450 nm, we can notice that a charge is transferred from the a_{1u} orbital of porphyrin unit A to the $(e_{gy}+e_{gx})/\sqrt{2}$ orbital of porphyrin unit B as depicted in Figure 9. When θ becomes less than 90°, the separation of the two terms cannot be preserved. Mixing of the excitonic and charge-resonance characters is expressed as simple equations as shown in Table 5. This illustrates that the excitonic transition is not only of excitonic character but also of charge-resonance character and vice-versa. Thus we can still witness that the RR enhancement of some vibrational modes of S1 by excitation at the charge-resonance band is similar to that by excitation at the well-separated excitonic band.

In addition to the effect of mixing between electronic transitions, the change of the depolarization ratios of the RR bands with a decrease of the dihedral angle should be addressed. The totally symmetric A_1 modes in D_{2d} symmetry group (A modes in D_2 group) would have ρ values of ca. 0.3 such as in Z2.[24] The intermediate value between zero (polarized) and 0.75 (totally depolarized) is caused by the symmetry tensor of $\alpha_{xx}^\circ = \alpha_{yy}^\circ \neq \alpha_{zz}^\circ$ and $\alpha_{xy}^\circ = \alpha_{yz}^\circ = \alpha_{zx}^\circ = 0$. The effect by symmetry reduction from D_{2d} to D_2 can be illustrated by representing the tensor components as $\alpha_{xx} = \alpha_{xx}^\circ - \delta$ and $\alpha_{yy} = \alpha_{xx}^\circ + \delta$ with $-1 \leq \delta/\alpha_{xx} \leq 1$. With the same parameter giving $\rho = 0.3$ in D_{2d} symmetry, the ρ value in D_2 symmetry varies from 0.3 to around 0.45. This explains the increased depolarization ratios of some RR bands with A_1 symmetry up to 0.5 as shown in Table 2. From the depolarization ratio values of the 1490 and 1578 cm^{-1} bands reaching up to 0.71 and 0.79, respectively, these bands can be assigned as the depolarized modes, which gain their intensities followed by the symmetry reduction from D_{2d} to D_2. We could also observe, even if very weak, similarly large values close to 0.75 in the RR spectrum of S10 for these bands.

Resonance Raman Enhancement. RR spectroscopy has been utilized to characterize the different electronic properties of optical transitions.[15−20] Asher and Sauer have worked out the rules for the vibrational enhancement by excitation within a particular type of electronic transition, especially for a porphyrin $\pi-\pi^*$ transition and a porphyrin-to-metal charge-transfer transition.[15] The Albrecht's B term depends on the vibronic coupling integral, $\langle e|\partial H/\partial Q_a|s\rangle$, which determines the spatial properties between two excited states. This integral is described by the transition density,[31,32]

$$\langle e|\partial H/\partial Q_a|s\rangle = \langle e|G|s\rangle = \int \langle e|\rho(r)|s\rangle G(r)\, dr$$

where $\langle e|\rho(r)|s\rangle$ is the transition density[33−35] representing the spatial overlap of $|e\rangle$ and $|s\rangle$. As Albrecht has pointed out, the mixed electronic states must lie within the same region of the molecule for vibronic mixing to occur.

In our case, charge transfer occurs between porphyrin rings, and the excitonic transitions lying closely are regarded to involve the vibronic interaction. For coupling of the CT_{1Z} transition (ca. 450 nm) with the nearby strong excitonic transitions, the EX_{2Z} and EX_{2Y} (or EX_{2X}) are possible. The transition density between the CT_{1Z} and EX_{2Z} becomes

$$\begin{aligned}\langle CT_{1Z}|\rho(r)|EX_{2Z}\rangle \approx \\ -[\langle a_{1u}{}^A(e_{gy}+e_{gx})^B|\rho(r)|a_{1u}{}^A(e_{gy}+e_{gx})^A\rangle + \\ \langle a_{1u}{}^A(e_{gy}+e_{gx})^B|\rho(r)|a_{1u}{}^B(e_{gy}+e_{gx})^B\rangle + \\ \langle a_{1u}{}^B(e_{gy}+e_{gx})^A|\rho(r)|a_{1u}{}^A(e_{gy}+e_{gx})^A\rangle + \\ \langle a_{1u}{}^B(e_{gy}+e_{gx})^A|\rho(r)|a_{1u}{}^B(e_{gy}+e_{gx})^B\rangle]/4\end{aligned}$$

For coupling between the CT_{1Z} and EX_{2Y}/EX_{2X}

$$\begin{aligned}\langle CT_{1Z}|\rho(r)|EX_{2Y} \text{ or } EX_{2X}\rangle \approx \\ [\langle a_{1u}{}^A(e_{gy}+e_{gx})^B|\rho(r)|a_{1u}{}^A(e_{gy}-e_{gx})^A\rangle \pm \\ \langle a_{1u}{}^A(e_{gy}+e_{gx})^B|\rho(r)|a_{2u}{}^B(e_{gy}+e_{gx})^B\rangle + \\ \langle a_{1u}{}^B(e_{gy}+e_{gx})^A|\rho(r)|a_{2u}{}^A(e_{gy}+e_{gx})^A\rangle \pm \\ \langle a_{1u}{}^B(e_{gy}+e_{gx})^A|\rho(r)|a_{1u}{}^B(e_{gy}-e_{gx})^B\rangle]/4\end{aligned}$$

These integrals illustrate that the region of maximum spatial overlap will occur in the position where the a_{1u} and $(e_{gy}+e_{gx})/\sqrt{2}$ orbitals are occupied. It is also anticipated that if a proper symmetry condition is satisfied, for instance, by symmetry degradation from D_{2d} to D_2, all three excitonic transitions are possibly coupled with the charge-transfer transition relying on the magnitude of spatial overlap. Considering that the a_{1u} and

TABLE 4: MO Description of S*N*s when $\theta = 90^\circ$ (D_{2d})

axis	eigenfunction[a]	energy[b]	symmetry	ΔE (eV)[c]	observed (nm)
Z	$CT_{1Z} = CT_{1+}{}^{+}$	$E - \delta$	$B_1(B_2)$[d]	3.07 (3.03)[e]	450
	$CT_{2Z} = CT_{2-}{}^{+}$	$E - \delta$	$B_1(A_2)$	3.14 (3.33)	
	$EX_{1Z} = \{Q_{x'}{}^{A} + Q_{x'}{}^{B}\}/2^{1/2}$	$E + \delta - 2\alpha$	$B_1(B_2)$	1.81 (1.76)	650
	$EX_{2Z} = \{B_{x'}{}^{A} + B_{x'}{}^{B}\}/2^{1/2}$	$E + \delta + 2\alpha$	$B_1(B_2)$	2.85 (2.70)	450
Y	$CT_{1Y} = CT_{1-}{}^{+}$	$E - \delta'$	E (B_2)	2.87 (2.82)	
	$CT_{2Y} = CT_{2+}{}^{+}$	$E - \delta'$	E (B_2)	3.34 (3.46)	
	$EX_{1Y} = \{Q_{y'}{}^{A} + Q_{y'}{}^{B}\}/2^{1/2}$	$E + \delta' + 2\alpha'$	E (B_2)	1.82 (1.77)	650
	$EX_{2Y} = \{B_{y'}{}^{A} + B_{y'}{}^{B}\}/2^{1/2}$	$E + \delta' - 2\alpha'$	E (B_2)	3.17 (3.12)	415
X	$CT_{1X} = CT_{1-}{}^{-}$	$E - \delta''$	E (B_3)	3.07 (2.80)	
	$CT_{2X} = CT_{2+}{}^{-}$	$E - \delta''$	E (B_3)	3.34 (3.36)	
	$EX_{1X} = \{Q_{y'}{}^{A} - Q_{y'}{}^{B}\}/2^{1/2}$	$E + \delta'' + 2\alpha''$	E (B_3)	1.82 (1.81)	650
	$EX_{2X} = \{B_{y'}{}^{A} - B_{y'}{}^{B}\}/2^{1/2}$	$E + \delta'' - 2\alpha''$	E (B_3)	3.17 (3.05)	415

[a] $Q_{x'}$, $B_{x'} = (B_x - B_y)/\sqrt{2} = \{a_{2u}(e_{gy} - e_{gx}) \pm a_{1u}(e_{gy} + e_{gx})\}/2$; $B_{y'}$, $Q_{x'} = (B_x + B_y)/\sqrt{2} = \{a_{2u}(e_{gy} + e_{gx}) \pm a_{1u}(e_{gy} - e_{gx})\}/2$; Q_x, $B_x = [(a_{2u}e_{gy}) \pm (a_{1u}e_{gx})]/\sqrt{2}$; B_y, $Q_y = [(a_{2u}e_{gx}) \pm (a_{1u}e_{gy})]/\sqrt{2}$; $CT_{1+}{}^{+} = \{a_{1u}{}^{A}(e_{gx}{}^{B} + e_{gy}{}^{B}) + a_{1u}{}^{B}(e_{gx}{}^{A} + e_{gy}{}^{A})\}/2$; $CT_{2-}{}^{+} = \{a_{2u}{}^{A}(e_{gx}{}^{B} - e_{gy}{}^{B}) + a_{2u}{}^{B}(e_{gx}{}^{A} - e_{gy}{}^{A})\}/2$; $CT_{1-}{}^{+} = \{a_{1u}{}^{A}(e_{gx}{}^{B} - e_{gy}{}^{B}) + a_{1u}{}^{B}(e_{gx}{}^{A} - e_{gy}{}^{A})\}/2$; $CT_{2+}{}^{+} = \{a_{2u}{}^{A}(e_{gx}{}^{B} + e_{gy}{}^{B}) + a_{2u}{}^{B}(e_{gx}{}^{A} + e_{gy}{}^{A})\}/2$; $CT_{1-}{}^{-} = \{a_{1u}{}^{A}(e_{gx}{}^{B} - e_{gy}{}^{B}) - a_{1u}{}^{B}(e_{gx}{}^{A} - e_{gy}{}^{A})\}/2$; $CT_{2+}{}^{-} = \{a_{2u}{}^{A}(e_{gx}{}^{B} + e_{gy}{}^{B}) - a_{2u}{}^{B}(e_{gx}{}^{A} + e_{gy}{}^{A})\}/2$. [b] $\alpha = {}^1/_2(a_{1u}{}^{A}(e_{gx}{}^{A} + e_{gy}{}^{A})|a_{2u}{}^{A}(e_{gx}{}^{A} - e_{gy}{}^{A})) + {}^1/_2(a_{1u}{}^{A}(e_{gx}{}^{A} + e_{gy}{}^{A})|a_{2u}{}^{B}(e_{gx}{}^{B} - e_{gy}{}^{B}))$; $\delta = -{}^1/_4(a_{1u}{}^{A}a_{1u}{}^{A}|(e_{gx}{}^{A} + e_{gy}{}^{A})(e_{gx}{}^{A} + e_{gy}{}^{A})) + {}^1/_4(a_{1u}{}^{A}a_{1u}{}^{A}|(e_{gx}{}^{B} + e_{gy}{}^{B})(e_{gx}{}^{B} + e_{gy}{}^{B})) + {}^1/_2(a_{1u}{}^{A}(e_{gx}{}^{A} + e_{gy}{}^{A})|a_{1u}{}^{A}(e_{gx}{}^{A} + e_{gy}{}^{A})) + {}^1/_2(a_{1u}{}^{A}(e_{gx}{}^{A} + e_{gy}{}^{A})|a_{1u}{}^{B}(e_{gx}{}^{B} + e_{gy}{}^{B}))$; $\alpha' = {}^1/_2(a_{1u}{}^{A}(e_{gx}{}^{A} - e_{gy}{}^{A})|a_{2u}{}^{A}(e_{gx}{}^{A} + e_{gy}{}^{A})) \pm {}^1/_2(a_{1u}{}^{A}(e_{gx}{}^{A} - e_{gy}{}^{A})|a_{2u}{}^{B}(e_{gx}{}^{B} + e_{gy}{}^{B}))$; δ', $\delta'' = -{}^1/_4(a_{1u}{}^{A}a_{1u}{}^{A}|(e_{gx}{}^{A} - e_{gy}{}^{A})(e_{gx}{}^{A} - e_{gy}{}^{A})) + {}^1/_4(a_{1u}{}^{A}a_{1u}{}^{A}|(e_{gx}{}^{B} - e_{gy}{}^{B})(e_{gx}{}^{B} - e_{gy}{}^{B})) + {}^1/_2(a_{1u}{}^{A}(e_{gx}{}^{A} - e_{gy}{}^{A})|a_{1u}{}^{A}(e_{gx}{}^{A} - e_{gy}{}^{A})) \pm {}^1/_2(a_{1u}{}^{A}(e_{gx}{}^{A} - e_{gy}{}^{A})|a_{1u}{}^{B}(e_{gx}{}^{B} - e_{gy}{}^{B}))$ [c] Excitation energy obtained by INDO/S−SCI calculations. [d] Symmetry notations under D_{2d} symmetry point group. [e] Transition energies calculated when $\theta = 60^\circ$.

TABLE 5: Change of the Transition Property by Dihedral Angle ($D_{2d} \rightarrow D_2$ Symmetry)

axis	D_{2d}	D_2[a,b]	observed (nm)
Z	$CT_{1Z} = CT_{1+}{}^{+}$	$CT_{1Z} = \{(1 + \lambda_Z{}^{+})[Q_{x'}{}^{A} + Q_{x'}{}^{B}] + (1 - \lambda_Z{}^{+})[CT_{1+}{}^{+} - CT_{2-}{}^{+}]\}/2\sqrt{1 + \lambda_Z{}^{+2}}$	450
	$CT_{2Z} = CT_{2-}{}^{+}$	$CT_{2Z} = \{(1 + \eta_Z{}^{-})[-B_{x'}{}^{A} - B_{x'}{}^{B}] + (1 - \eta_Z{}^{-})[CT_{1+}{}^{+} + CT_{2-}{}^{+}]\}/2\sqrt{1 + \eta_Z{}^{-2}}$	390
	$EX_{1Z} = \{Q_{x'}{}^{A} + Q_{x'}{}^{B}\}/2^{1/2}$	$EX_{1Z} = \{(1 + \lambda_Z{}^{-})[Q_{x'}{}^{A} + Q_{x'}{}^{B}] + (1 - \lambda_Z{}^{-})[CT_{1+}{}^{+} - CT_{2-}{}^{+}]\}/2\sqrt{1 + \lambda_Z{}^{-2}}$	650
	$EX_{2Z} = \{B_{x'}{}^{A} + B_{x'}{}^{B}\}/2^{1/2}$	$EX_{2Z} = \{(1 + \eta_Z{}^{+})[-B_{x'}{}^{A} - B_{x'}{}^{B}] + (1 - \eta_Z{}^{+})[CT_{1+}{}^{+} + CT_{2-}{}^{+}]\}/2\sqrt{1 + \eta_Z{}^{+2}}$	480
Y	$CT_{1Y} = CT_{1-}{}^{+}$	$CT_{1Y} = \{(1 + \lambda_Y{}^{-})[B_{y'}{}^{A} + B_{y'}{}^{B}] + (1 - \lambda_Y{}^{-})[-CT_{1-}{}^{+} + CT_{2+}{}^{+}]\}/2\sqrt{1 + \lambda_Y{}^{-2}}$	450
	$CT_{2Y} = CT_{2+}{}^{+}$	$CT_{2Y} = \{(1 + \eta_Y{}^{+})[Q_{y'}{}^{A} + Q_{y'}{}^{B}] + (1 - \eta_Y{}^{+})[CT_{1-}{}^{+} + CT_{2+}{}^{+}]\}/2\sqrt{1 + \eta_Y{}^{+2}}$	390
	$EX_{1Y} = \{Q_{y'}{}^{A} + Q_{y'}{}^{B}\}/2^{1/2}$	$EX_{1Y} = \{(1 + \eta_Y{}^{-})[Q_{y'}{}^{A} + Q_{y'}{}^{B}] + (1 - \eta_Y{}^{-})[CT_{1-}{}^{+} + CT_{2+}{}^{+}]\}/2\sqrt{1 + \eta_Y{}^{-2}}$	650
	$EX_{2Y} = \{B_{y'}{}^{A} + B_{y'}{}^{B}\}/2^{1/2}$	$EX_{2Y} = \{(1 + \lambda_Y{}^{+})[B_{y'}{}^{A} + B_{y'}{}^{B}] + (1 - \lambda_Y{}^{+})[-CT_{1-}{}^{+} + CT_{2+}{}^{+}]\}/2\sqrt{1 + \lambda_Y{}^{+2}}$	420
X	$CT_{1X} = CT_{1-}{}^{-}$	$CT_{1X} = CT_{1-}{}^{-}$	
	$CT_{2X} = CT_{2+}{}^{-}$	$CT_{2X} = CT_{2+}{}^{-}$	390
	$EX_{1X} = \{Q_{y'}{}^{A} - Q_{y'}{}^{B}\}/2^{1/2}$	$EX_{1X} = \{Q_{y'}{}^{A} - Q_{y'}{}^{B}\}/2^{1/2}$	650
	$EX_{2X} = \{B_{y'}{}^{A} - B_{y'}{}^{B}\}/2^{1/2}$	$EX_{2X} = \{B_{y'}{}^{A} - B_{y'}{}^{B}\}/2^{1/2}$	420

[a] $\lambda_Z{}^{\pm} = [2\beta \pm \sqrt{(4\beta^2 + (\alpha - \delta)^2}]/(\delta - \alpha)$, and $\eta_Z{}^{\pm} = [2\beta \pm \sqrt{(4\beta^2 + (\alpha + \delta)^2}]/(\delta + \alpha)$. [b] $\lambda_Y{}^{\pm} = [2\beta \pm \sqrt{(4\beta^2 + (\alpha' - \delta')^2}]/(\delta' - \alpha')$, and $\eta_Y{}^{\pm} = [2\beta \pm \sqrt{(4\beta^2 + (\alpha' + \delta')^2}]/(\delta' + \alpha')$.

$(e_{gy} + e_{gx})/\sqrt{2}$ orbitals have large electron densities at C_α and C_β, we can differentiate the vibrational modes involving the vibronic coupling between the charge-resonance transition and the nearby excitonic transitions. The vibrational modes related to vibronic coupling would involve the movement of C_α and C_β carbons, for instance, $\nu(C_\alpha C_\beta)$ and $\nu(C_\beta C_\beta)$.

The Franck−Condon scattering (the Albrect A-term) also predicts the RR enhancement of the vibrations involving the C_α and C_β movement. Because the charge-resonance mainly occurs in the porphyrin macrocycle, the maximum change in the electronic configuration of the excited state vs. the ground state occurs within the porphyrin macrocycle. Concurrently, the equilibrium nuclear configuration shows its maximum change within the macrocycle. This results in different potentials within the Hamiltonian for the excited state compared to the ground state. This means that

$$\langle gi|ev\rangle\langle ev|gj\rangle \neq \delta_{ij}$$

where

$$A = \sum_{v}\left[\frac{\langle g|R_\sigma|e\rangle\langle g|R_\rho|e\rangle}{\nu_{ev,gi} - \nu_o + i\Gamma_e}\right]\langle gi|ev\rangle\langle ev|gj\rangle^{36}$$

and RR intensity can be derived from the A term.

We have noted the appearance of depolarized RR bands by 457.9 nm excitation. Possible symmetries of the vibrations giving depolarized Raman tensors are B_1, B_2, and E in D_{2d} group (A, B_1, and B_2/B_3 in D_2 group, respectively). For the vibronic coupling integral, $\langle CT_{1Z}|\partial H/\partial Q_a|EX\rangle$, to be nonzero, the direct product of the three terms in the integral should have a totally symmetric component. Since the symmetry of the CT_{1Z} transition is the B_2 in D_{2d} symmetry group, the product with the EX_{2Z} (B_2 symmetry) results in the totally symmetric A_1 representation. Thus, only the A_1 vibrational modes are resonantly enhanced. The product with the EX_{2Y} or EX_{2X} predicts the E symmetry modes, which makes the coupling integral nonzero. This argument is supported by the two depolarized RR bands at 1490 and 1578 cm^{-1}. This also reflects that the EX_{2Y} and EX_{2X} transitions contribute partially to the enhancement of the depolarized RR bands through vibronic coupling while the EX_{2Z} transition explains the A_1 mode enhancement. As for the A_1 mode enhancement, the effect of exciton and charge transfer mixing, as mentioned above, is not underestimated but regarded to contribute together.

In assigning the RR modes resonantly enhanced by excitation at the charge-resonance transition, we can provide a consistent mode assignment by the fact that the a_{1u} and $(e_{gy} + e_{gx})/\sqrt{2}$ orbitals have large electron densities at C_α and C_β, and thus

vibrations involving $\nu(C_\alpha C_\beta)$ and $\nu(C_\beta C_\beta)$ will be enhanced significantly. The 1490 and 1578 cm^{-1} bands are assigned to originate from the ν_{11} ($\nu(C_\beta C_\beta) + \delta(C_\beta H)$) and ϕ_4'' ($\nu(C_m - C_{Ph}) + \nu_{8a}(Ph) + \nu(C_\beta C_\beta)$) modes of porphyrin monomer, respectively. The symmetries of the ν_{11} and ϕ_4'' modes in porphyrin monomer unit are B_{1g} and E_u under D_{4h} symmetry group, respectively. The 1578 cm^{-1} band seems to comprise the closely lying ϕ_4 and ϕ_4'' modes. The other RR bands that are enhanced by excitation at the charge-resonance transition are similarly assigned such as the 1519, 1444, and 1023 cm^{-1} bands to the ν_{38} and ν_3 modes with $\nu(C_\alpha C_m) + \nu(C_\beta C_\beta)$, and the ν_{22} mode with $\nu(C_\alpha C_\beta) + \nu(NC_\alpha)$, respectively. For the assignment of the 1023 cm^{-1} band, ambiguities still remain due to the closely lying Raman bands such as the ν_{15} and ν_{30} modes.[23] These Raman bands show high sensitivity to the charge-resonance character. The diminishment of the ν_8 mode at 387 cm^{-1} involving mostly $\nu(NM) + \delta(C_\alpha NC_\alpha) + \nu(C_\alpha C_m)$ motions is consistent with the other observations because this mode has very large polarizability as shown by a strong enhancement by excitation at 488.0 nm. It is consistent that most of the RR bands of A_1 symmetry with considerable intensities also contain the $\nu(C_\alpha C_\beta)$ and $\nu(C_\beta C_\beta)$ components. Some of the RR bands at 1543, 1351, 1188, 1074, and 1005 cm^{-1} are assigned to the ν_2, ν_4, ν_{51}, ν_9, and ν_6 modes, which involve the $\nu(C_\alpha C_\beta)$ or $\nu(C_\beta C_\beta)$ vibrations. The enhancement of the triple RR bands at around 660 cm^{-1} is attributed to the contribution of the C_α movement since these Raman modes involve the $\delta(C_\alpha C_m C_\alpha)$ vibration at the linking site of the porphyrin dimer. Nonnegligible enhancement of the 173 and 226 cm^{-1} bands that have no $\nu(C_\alpha C_\beta)$ and $\nu(C_\beta C_\beta)$ components is ascribed to the phenyl ring rotation caused by the short linking chain. The same argument can be applied to the ν_{27} mode at 1290 cm^{-1} having $\nu(NC_\alpha) + \nu(C_m C_{phenyl})$ vibration.

Fluorescence Decay Behavior. At this point it is necessary to mention the double exponential decay behavior of the fluorescence decay (Table 1). The time constants of the two decay components are different by roughly three times. This seems to indicate the existence of two different emission states lying nearly degenerate. A certain CT transition may serve as an additional decay route for the fast decay component. However, no CT or CR transitions but only Q-bands exist in this region. Due to the small oscillator strength, the excitonic interaction between Q-bands is very weak, resulting in nearly degenerate states. Examining carefully the trends of the Q-band energies with a change of the dihedral angle, we notice that the one with *Z*-direction is lowest in energy, and the other degenerate ones with *Y*- and *X*-directions are a little higher in energy when $\theta = 90°$. As the dihedral angle decreases, the ones with *Z*- and *Y*-directions shift to lower energy reaching almost the degenerate states while the one with *X*-direction lies higher than the others. Thus the two Q-states may emit light in a competitive manner. The Q-state with *Y*-direction can be mixed with the CT_{2Y} transition as shown in Table 5. If we consider that the CT_{2Y} transition is largely enhanced with a decrease of the dihedral angle, there will be some vibronically activated vibrations. The activated vibrations may play a major role in accelerating the decay of the Q-state emission with *Y*-direction.

V. Conclusion

The unusual proximity of the porphyrin units through meso-meso direct linkage and the dihedral angle change between the porphyrin units exhibit new electronic absorptions due to strong orbital interactions. New charge-resonance transitions at 390 and 450 nm and a large red shift of the excitonic Soret transitions at 415 and 450 nm up to 420 and 480 nm are caused by the increased orbital interactions between the porphyrin planes with a decrease of the dihedral angle. With the aid of MO calculations, considerable mixing between the charge-resonance and excitonic transitions was inferred, which was evidenced by the excitonic nature of the RR enhancement by excitation at the charge-resonance transition. It was also found that most orbital overlap occurs at the C_α and C_β positions in the charge-resonance transition and thus the vibration modes involving the $\nu(C_\alpha C_\beta)$ and $\nu(C_\beta C_\beta)$ motions are dominantly enhanced by excitation at the charge-resonance transition. The mixing between electronic states is tentatively proposed to be responsible for the heterogeneity in the fluorescence decay. Collectively, RR spectroscopy was successfully applied to characterize the charge-resonance and excitonic transitions in relation to the molecular structures in the directly linked porphyrin dimers.

Acknowledgment. The work at Yonsei University has been financially supported by the National Creative Research Initiatives Program of the Ministry of Science & Technology of Korea. The work at Kyoto was supported by CREST (Core Research for Evolutional Science and Technology) of Japan Science and Technology Corporation (JST). We also thank Mr. Y. Matsuzaki for his help in our MO calculations.

References and Notes

(1) (a) Wagner, R. W.; Lindsey, J. S. *J. Am. Chem. Soc*. **1994**, *116*, 9759. (b) Prathapan, S.; Johnson, T. E.; Lindsey, J. S. *J. Am. Chem. Soc.* **1993**, *115*, 7519. (c) Wagner, R. W.; Lindsey, J. S.; Seth, J.; Palaniappan, V.; Bocian, D. F. *J. Am. Chem. Soc.* **1996**, *118*, 3996.

(2) (a) Gosztola, D.; Yamada, H.; Wasielewski, M. R. *J. Am. Chem. Soc.* **1995**, *117*, 2041. (b) Debreczeny, M. P.; Svec, W. A.; Marsh, E. M.; Wasielewski, M. R. *J. Am. Chem. Soc*. **1996**, *118*, 8174. (c) Debreczeny, M. P.; Svec, W. A.; Wasielewski, M. R. *Science* **1996**, *274*, 584.

(3) (a) Beljonne, D.; O'Keefe, G. E.; Hamer, P. J.; Friend, R. H.; Anderson, H. L.; Bredas, J. L. *J. Chem. Phys.* **1997**, *106*, 9439. (b) Karki, L.; Vance, F. W.; Hupp, J. T.; LeCours, S. M.; Therien, M. J. *J. Am. Chem. Soc*. **1998**, *120*, 2606. (c) Joran, A. D.; Leland, B. A.; Felker, P. M.; Zewail, A. H.; Hopfield, J. J.; Dervan, P. B. *Nature* **1987**, *327*, 508. (d) Wasielewski, M. R.; Gaines, G. L., III; Wiederrecht, G. P.; Svec, W. A.; Niemczyk, M. P. *J. Am. Chem. Soc*. **1993**, *115*, 10442. (e) Osuka, A.; Marumo, S.; Mataga, N.; Taniguchi, S.; Okada, T.; Yamazaki, I.; Nishimura, Y.; Ohno, T.; Nozaki, K. *J. Am. Chem. Soc*. **1996**, *118*, 155. (f) Strachan, J.-P.; Gentemann, S.; Seth, J.; Kalsbeck, W. A.; Lindsey, J. S.; Holten, D.; Bocain, D. F. *J. Am. Chem. Soc*. **1997**, *119*, 11191.

(4) (a) Wasielewski, M. R. *Chem. Rev*. **1992**, *94*, 435. (b) Gust, D.; Moore, T. A.; Moore, A. L. *Acc. Chem. Res*. **1993**, *26*, 198. (c) Speiser, S. *Chem. Rev*. **1996**, *96*, 1953. (d) Chou, J.; Kosal, M. E.; Nalwa, H. S.; Rakow, N. A.; Suslick, K. S. In *The Porphyrin Handbook*; Kadish, K. M., Smith, K. M., Guilard, R., Eds.; Academic Press: New York, 2000; Vol. 6, p 43.

(5) (a) Lin, V. S.-Y.; DiMagno, S. G.; Therien, M. J. *Science* **1994**, *264*, 1105. (b) Lin, V. S.-Y.; Therien, M. J. *Chem.-Eur. J*. **1995**, *1*, 645.

(6) (a) Arnold, D. P.; Nitschinsk, L. J. *Tetrahedron Lett.* **1992**, *48*, 8781. (b) Arnold, D. P.; Heath, G. A.; James, D. A. *J. Por. Phthl*. **1999**, *3*, 5. (c) Arnold, D. P.; Nitschinsk, L. *Tetrahedron Lett.* **1993**, *34*, 693. (d) Anderson, H. L. *Inorg. Chem*. **1994**, *33*, 972. (e) Anderson, H. L. *Chem. Commun*. **1999**, 2323.

(7) (a) Vicente, M. G. H.; Smith, K. M. *J. Org. Chem.* **1991**, *56*, 4407. (b) Vicente, M. G. H.; Jaquinod, L.; Smith, K. M. *Chem. Commun*. **1999**, 1771.

(8) (a) Burrell, A. K.; Officer, D.; Reid, D. *Angew. Chem., Int. Ed. Engl*. **1995**, *34*, 900. (b) Burrell, A. K.; Officer, D. L. *Synth. Lett*. **1998**, 1297.

(9) (a) Osuka, A.; Liu, B.-L.; Maruyama, K. *Chem. Lett*. **1993**, 949. (b) Osuka, A.; Maruyama, K.; Mataga, N.; Asahi, T.; Yamazaki, I.; Tamai, N. *J. Am. Chem. Soc*. **1990**, *112*, 4958. (c) Osuka, A.; Nakajima, S.; Maruyama, K.; Mataga, N.; Asahi, T.; Yamazaki, I.; Nishimura, Y.; Ohno, T.; Nozaki, K. *J. Am. Chem. Soc*. **1993**, *115*, 4577. (d) Osuka, A.; Maruyama, K. *J. Am. Chem. Soc*. **1988**, *110*, 4454. (e) Osuka, A.; Maruyama, K.; Yamazaki, I.; Tamai, N. *J. Chem. Soc., Chem. Commun.* **1988**, 1243. (f) Osuka, A.; Maruyama, K.; Yamazaki, I.; Tamai, N. *Chem. Phys. Lett*. **1990**, *165*, 392.

(10) (a) Ponomarev, G. V.; Borovkov, V.; Sugiura, K.; Sakata, Y.; Shul'ga, A. *Tetrahedron Lett*. **1993**, *34*, 2153. (b) Ponomarev, G.; Borovkov,

V.; Shul'ga, A.; Sakata, Y. *J. Chem. Soc., Chem. Commun*. **1994**, 1927. (c) Senge, M. O.; Gerzevske, K.; Vicente, M. G. H.; Forsyth, T.; Smith, K. M. *Angew. Chem., Int. Ed. Engl.* **1993**, *32*, 750. (d) Senge, M. O.; Vicente, M. G. H.; Gerzevske, K.; Forsyth, T.; Smith, K. M. *Inorg. Chem*. **1994**, *33*, 5625. (e) Higuchi, H.; Takeuchi, M.; Ojima, J. *Chem. Lett*. **1996**, 593. (f) Sugiura, K.; Tanaka, H.; Matsumoto, T.; Kawai, T.; Sakata, Y. *Chem. Lett*. **1999**, 1193.

(11) (a) Sessler, J. L.; Johnson, M. R. *Angew. Chem., Int. Ed. Engl*. **1987**, *26*, 678. (b) Sessler, J. L.; Capuano, V. L.; Harriman, A. *J. Am. Chem. Soc*. **1993**, *115*, 4618. (c) Brun, A. M.; Harriman, A.; Heitz, V.; Sauvage, J.-P. *J. Am. Chem. Soc*. **1991**, *113*, 8657. (d) Härberle, T.; Hirsch, J.; Pöllinger, F.; Heitele, H.; Michel-Beyerle, M. E.; Anders, C.; Döhling, A.; Krieger, C.; Rückemann, A.; Staab, H. A. *J. Phys. Chem.* **1996**, *100*, 18269. (e) Staab, H. A.; Carell, T. *Angew. Chem., Int. Ed. Engl.* **1994**, *33*, 1466.

(12) Yoshida, N.; Shimidzu, H.; Osuka, A. *Chem. Lett*. **1998**, 55.

(13) Aratani, N.; Osuka, A.; Kim, Y. H.; Jeong, D. H.; Kim, D. *Angew. Chem., Int. Ed.* **2000**, *39*, 1458.

(14) Yoshida, N.; Osuka, A. *Org. Leet*. **2002**, *19*, 2963.

(15) Asher, S.; Sauer, K. *J. Chem. Phys.* **1976**, *64*, 4115.

(16) Yu, N.-T.; Tsubaki, M. *Biochem*. **1980**, *19*, 4647.

(17) Bjerre, N.; Bates, J. B. *J. Chem. Phys*. **1983**, *78*, 2133.

(18) McMahon, R. J.; Forcé, K.; Patterson, H. H.; Wrighton, M. S. *J. Am. Chem. Soc.* **1988**, *110*, 2670.

(19) Martin, P. C.; Arnold, J.; Bocian, D. F. *J. Phys. Chem*. **1993**, *97*, 1332.

(20) Ohno, S.; Kaizu, Y.; Kobayashi, H. *J. Chem. Phys*. **1993**, *99*, 4128.

(21) Lee, M.; Kim, D. *J. Opt. Soc. Korea* **1990**, *1*, 52.

(22) Kim, Y. H.; Jeong, D. H.; Kim, D.; Jeoung, S. C.; Cho, H. S.; Kim, S. K.; Aratani, N.; Osuka, A. *J. Am. Chem. Soc*. **2001**, *123*, 76.

(23) Li, X.-Y.; Czernuszewicz, R. S.; Kincaid, J. R.; Su, Y. O.; Spiro, T. G. *J. Phys. Chem*. **1990**, *94*, 31.

(24) Jeong, D. H.; Yoon, M.-C.; Jang, S. M.; Kim, D.; Cho, D. W.; Yoshida, N.; Aratani, N.; Osuka, A. *J. Phys. Chem. A* **2002**, *106*, 2359.

(25) Ohta, N.; Iwaki, Y.; Ito, T.; Yamazaki, Iwao.; Osuka, A. *J. Phys. Chem. B* **1999**, *103*, 11242.

(26) Gouterman, M. In *The Porphyrins*; Dolphin, D., Ed.; Academic Press: New York, 1978; Vol. III, pp 1−165.

(27) Bilsel, O.; Rodriguez, J.; Milan, S. N.; Gorlin, P. A.; Girolami, G. S.; Suslick, K. S.; Holten, D. *J. Am. Chem. Soc.* **1992**, *114*, 6528.

(28) Donohoe, R. J.; Duchowski, J. K.; Bocian, D. F. *J. Am. Chem. Soc*. **1988**, *110*, 6119.

(29) Duchowski, J. K.; Bocian, D. F. *J. Am. Chem. Soc*. **1990**, *112*, 3312.

(30) Perng, J.-H.; Duchowski, J. K.; Bocian, D. F. *J. Phys. Chem*. **1990**, *94*, 6684.

(31) Nurrel, J. N.; Pople, J. A. *Proc. Phys. Soc. London Sect. A* **1956**, *69*, 245.

(32) Longuet-Higgins, H. C. *Proc. R. Soc. London Ser. A* **1956**, *235*, 537.

(33) Albrecht, A. C. *J. Chem. Phys*. **1961**, *34*, 1476.

(34) Tang, J.; Albrecht, A. C. In *Raman Spectroscopy*; Szymanski, H. A., Ed.; Plenum: New York, 1971; Vol. II.

(35) Longuett-Higgins, H. C. *Proc. R. Soc. London Ser. A* **1956**, *235*, 537.

(36) Albrecht, A. C.; Hutley, M. C. *J. Chem. Phys.* **1971**, *55*, 4438.